(Received 29 September 2025, Accepted 4 November 2025, Scheduled 10 January 2026)

Frequency-Dependent Electromagnetic Response of Argon, Krypton, and Xenon Plasmas: A Theoretical and Simulation Study

Ayoub El Jaouhari[1,*], Abdelhak Missaoui[2], Moussa El Yahyaoui[1], Majid Rochdi[1], and Morad El Kaouini[1]

[1] *LMASI, Electromagnetism, Physics of Plasmas and Applications, Polydisciplinary Faculty of Nador, Mohammed First University, Nador 62700, Morocco*
[2] *Laboratory of Physics of Matter and Radiations, Faculty of Sciences, Mohammed First University, Oujda 60040, Morocco*

ABSTRACT: In this paper, the frequency-dependent electromagnetic response of argon, krypton, and xenon plasmas is investigated using a fluid approach, the Drude model and the Transfer Matrix Method (TMM). The key plasma properties, electron density, collision frequency, and plasma frequency, of a Capacitively Coupled Plasma (CCP) were obtained using a drift–diffusion fluid model within the COMSOL Multiphysics. These properties were then used to predict how the plasma would react to electromagnetic waves in the 0 to 200 gigahertz band. The obtained results demonstrate that the reflective and transmissive characteristics of each gas depend on its plasma frequency. Argon acts as an efficient reflector below 20 GHz and becomes highly transparent above 30 GHz. In contrast, Krypton maintains a strong reflection up to 85 GHz, while xenon remains reflective up to 140 GHz before it becomes transmissive. The observed differences are caused by the variations in each gas's plasma frequency and electron-neutral collision rates. The TMM results show excellent agreement with Finite-Difference Time-Domain (FDTD) simulations. The comparison between the two methods demonstrates that TMM is a faster and equally accurate approach for wideband electromagnetic analysis and for the design of adaptive plasma-based frequency-selective devices, including plasma antennas, plasma reflectors, and intelligent reflective surfaces (IRS).

1. INTRODUCTION

The concept that plasma properties can be modified to control electromagnetic wave reflection and transmission has attracted considerable research attention since the mid-20th century. One of the earliest to suggest this concept was Irving Langmuir, who conducted extensive research on plasma in the 1920s and 1930s [1]. Over the past two decades, research has shown that plasma can be used in different applications, such as plasma stealth [2], plasma antennas [3–7], plasma reflectors [8–12], and plasma filters [13].

From a technological perspective, several methods can be used to generate plasma. These methods include laser-initiated atmospheric discharges [14], DC/AC discharges [15], and high-frequency surface-wave plasmas [16]. However, the most widely used method for plasma generation is the Single-Frequency Capacitively Coupled Plasma (SF-CCP) [17, 18]. This technique uses the electrical breakdown of a neutral gas in the presence of an external ac electric field. Charge carriers, accelerated in the electric field, transfer their energy due to the collision between the charged particles and other particles in the plasma. Due to their low mass, the electrons undergo little loss in energy due to an elastic collision with the atoms or molecules and dissipate most of their energy in the inelastic collision.

The main methods for analyzing the interaction between plasma and electromagnetic waves for the theoretical calculation of reflection and transmission coefficients include the FDTD, Finite-Element Method (FEM), Frequency-Domain Finite-Difference (FDFD), and TMM. Among these, the TMM is considered relatively simple and flexible. However, there is a lack of literature comparing the transmission properties of three different gases using these methods. Cummer [19] evaluated different FDTD methods for modeling electromagnetic wave propagation in isotropic cold plasma. Yuan et al. [20] analyzed the influence of plasma parameters, such as electron density, plasma layer thickness, collision frequency, and electron temperature, on the absorption and reflection of THz waves using FDTD. Zhang et al. [21] developed a 2-D FDTD model to study the propagation of broadband plane waves across a re-entry plasma sheath, showing the effects of inhomogeneities on the associated EM signals. The work of Chen et al. [22] investigated the scattering of EM waves in time-varying spatially non-uniform plasmas sheaths using a 3-D FDTD algorithm, studying RCS variations and their effects on attenuation and scattering. The TMM, on the other hand, portends a complete satisfaction of reflection and transmission problems involving layered media, including plasmas with complex permittivity and conductivity. Yuan et al. [23] presented a plasma stealth model based on impedance matching of multiple dielectrics, which evidently showed that

* Corresponding author: Ayoub El Jaouhari (ayoub.eljaouhari@ump.ac.ma).

the thickness of a plasma sheath and the electron density were prime features in analysis of stealth efficiency. Hu et al. [24] presented the Scattering Matrix Method (SMM) to study the reflection, absorption, and transmission of EM waves through the non-uniform application of a magnetised plasma plate. They showed that both electron density and collision frequency were important factors in modifying these properties. Yang et al. [25] showed that the transmission coefficients could be determined by the antenna voltage standing wave ratio (VSWR) values and could be affected by the presence of a plasma sheath below the spacecraft. They pointed out that VSWR values would predict transmission loss, which indicates trouble in all transmission paths, without the necessity of employing feedback channels, thus constituting a considerable step in the matter of reducing electronic blackout for spacecraft. Liu et al. [26] investigated the transmission characteristics of EM waves in high-temperature plasma using TMM, noting negative conductivity and anomalous transmission phenomena, both of which could be the result of ad hoc adjustment of magnetic fields.

At very small length scales, typically below a few micrometers, classical continuum models may lose accuracy due to the significance of internal length parameters and non-local field interactions (known as "size effect"). Such "size effects" have been observed in mechanical [27] and magneto-mechanical [28] micro-structures, leading to the formulation of non-classical continuum theories. In this context, the conventional TMM can be extended to include higher-order gradient terms, leading to the so-called Non-Classical Transfer Matrix Method (NCTMM) [29]. The NCTMM accounts for internal length parameters, micro-rotations, and non-local stress or field couplings that are negligible in macroscopic materials. In the present work, the plasma slab has millimeter-scale dimensions and a uniform electron density, so the classical electromagnetic TMM is fully adequate. However, for future miniaturized plasma devices or plasma-on-chip configurations, incorporating NCTMM could provide a more accurate representation of size-dependent electromagnetic behavior.

The research presented in [19–25] has provided useful knowledge about plasma-electromagnetic interactions. However, these works typically focus on a single gas, which limits our understanding of the advantages of using one gas over another. Additionally, while some research has explored specific aspects in different domains, such as wireless communications using plasma, a comprehensive comparative analysis across different gases is often absent.

In this study, we have used a one-dimensional (1D) fluid model to simulate the plasma discharge. The plasma is confined in a dielectric tube with two parallel identical hollow electrodes separated by a few centimeters. The study aims to investigate general features of SF-CCP discharges operating at 1.5 Torr and driven by an applied AC voltage. Simulations are performed for three different gases: argon, krypton, and xenon. The steady-state solutions for charged-particle density, electron temperature, and collision frequency are calculated using COMSOL Multiphysics. For each ionized gas, we determine its ability to reflect and transmit electromagnetic waves by analyzing the reflection and transmission coefficients. Our novel comparative approach examines the electromagnetic response of argon, krypton, and xenon when exposed to an incident radio frequency (RF) wave, providing a detailed analysis of each gas's specific electromagnetic behavior according to its intrinsic properties. Furthermore, a combination of theoretical and simulation work on a plasma with controllable gas composition is presented to investigate how this affects plasma behaviour in various frequency domains. The primary focus of our research is to thoroughly investigate the phenomena of reflection and transmission in a homogeneous cold plasma surrounded by air using the TMM, by comparing the behaviour of argon, krypton, and xenon under identical conditions.

Beyond the fundamental analysis, this work provides a practical framework for the rapid and accurate prediction of plasma electromagnetic behaviour with minimal computational cost using TMM compared to FDTD methods. The findings will be helpful for the optimization of gas-based plasma systems and are directly useful for the design of plasma antennas, plasma reflectors, and new intelligent reflective surfaces (IRS), where tunable plasma properties will allow the realization of reconfigurable and adaptable electromagnetic properties.

The paper is structured as follows. Section 2 presents the RF discharge geometry and the theoretical model used to determine electron density and collision frequency for the argon, krypton, and xenon gases. Section 3 discusses the theory of plasma and electromagnetic wave interaction, considering reflection and transmission coefficients based on the Drude model and TMM. Section 4 contains the numerical results, and Section 5 concludes the present study.

2. PLASMA MODEL

2.1. Geometric Model of CCP Plasma

In this study, we consider a plasma confined within a glass chamber and maintained between two identical hollow electrodes, each 20 mm long, as shown in Figure 1. The electrodes have an inner radius of 2 mm and an outer radius of 3 mm, and are positioned 100 mm apart. The cathode is driven by an RF signal oscillating at a frequency of $f_d = 19$ KHz, while the anode is electronically grounded. These parameters were chosen to match the experimental conditions reported in [10], which serves to validate our results. The applied V_{rf} voltage has the form of:

$$V_{rf} = V_{\max} \sin(2\pi f_d t) \tag{1}$$

where $V_{\max}$ is the amplitude. Due to the symmetry of the two electrodes (symmetric area), the DC self-bias voltage is regarded as zero [30].

2.2. Theoretical Basis of the Plasma

To study plasma discharges, it is essential to determine the electron density (n_e) and electron-atom collision frequency (υ_c). Plasma discharge can be modeled using three main approaches [31]: statistical (or particle) models [32], fluid (or continuum) models [33], and hybrid models [34]. Each model

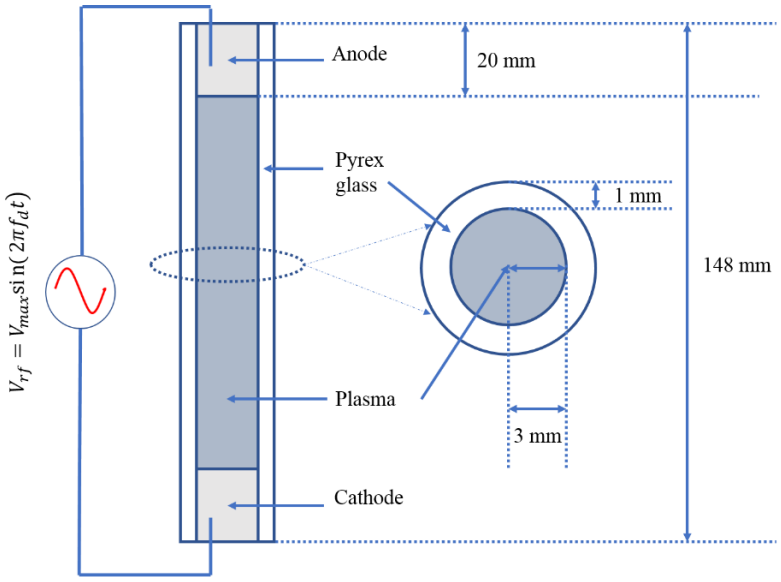

FIGURE 1. Schematic of plasma generation using the capacitively coupled plasma (CCP) method.

has specific advantages and drawbacks, making them suitable for different conditions.

In this paper, we have used the fluid model combined with a drift-diffusion approach to describe the transport of the different species (electrons, ions and atoms) in a CCP excited by a single radio frequency discharge. The plasma considered in this model contains electrons (e), positively charged ions (X^+), metastable atoms (X^*), and neutral atoms (X). The model is based on several assumptions, described in the following points:

I. In cold plasma, neutral atoms (X) constitute the dominant species. These atoms are uniformly distributed in the plasma, and using the ideal gas law, their density can be easily determined by knowing the gas pressure and its temperature.

II. Since ions are much heavier than electrons, they can only gain a small amount of energy from the applied field. However, the ions dissipate a large portion of their energy in collisions with electrons. As a result, ions have a substantially lower average energy than electrons. Consequently, we assume the ion temperature (T_i) equals the neutral gas temperature (T_g), and thus we omit the ion energy equation.

III. The general formula of the collision frequency υ_c, in the plasma is given by [35]:

$$\upsilon_c = \upsilon_{e-a} + \upsilon_{e-i} + \upsilon_{e-e} \tag{2}$$

where υ_{e-a}, υ_{e-i}, and υ_{e-e} are the electron-atom, electron-ion, and electron-electron collision frequency, respectively. If we consider a cold and weakly ionized plasma, we can neglect υ_{e-i} and υ_{e-e} compared to υ_{e-a}, and the Equation (2) becomes:

$$\upsilon_c \approx \upsilon_{e-a} = \sqrt{\frac{8}{\pi K_B m_e}}\left[(T_g)\times(P_g)\times\left(T_e^{0.5}\right)\times(Q_{e-a})\right] \tag{3}$$

where K_B is the Boltzmann constant, m_e electron mass, T_g the gas temperature, P_g the gas pressure, T_e the electron temperature, and Q_{e-a} the total electron-atom cross-section, which is given by:

$$Q_{e-a} = Q_{e-a}^{elas} + Q_{e-a}^{exci} + Q_{e-a}^{ioni} \tag{4}$$

where Q_{e-a}^{elas}, Q_{e-a}^{exci}, and Q_{e-a}^{ioni} are the elastic, excitation, and ionization electron-atom cross-section, respectively.

IV. The chemical reactions considered for the three different gases are presented in Tables 1, 2, and 3.

TABLE 1. Argon plasma chemical reactions [36].

Reaction	Formula	Type	$\Delta\varepsilon$ (eV)
1	e+Ar→e+Ar	Elastic	0
2	e+Ar→e+Ar*	Excitation	11.5
3	e+Ar→2e+Ar+	Ionization	−11.5

TABLE 2. Krypton plasma chemical reactions [36].

Reaction	Formula	Type	$\Delta\varepsilon$ (eV)
1	e+Kr→e+Kr	Elastic	6.50e-6
2	e+Kr→e+Kr*	Excitation	9.915
3	e+Kr→2e+Kr+	Ionization	13.996

TABLE 3. Xenon plasma chemical reactions [36].

Reaction	Formula	Type	$\Delta\varepsilon$ (eV)
1	e+Xe→e+Xe	Elastic	4.20e-6
2	e+Xe→e+Xe*	Excitation	8.310
3	e+Xe→2e+Xe+	Ionization	12.12

The model takes into consideration the collisions between electrons (e) and neutral particles (X) involving elasticity, excitation, and ionization.

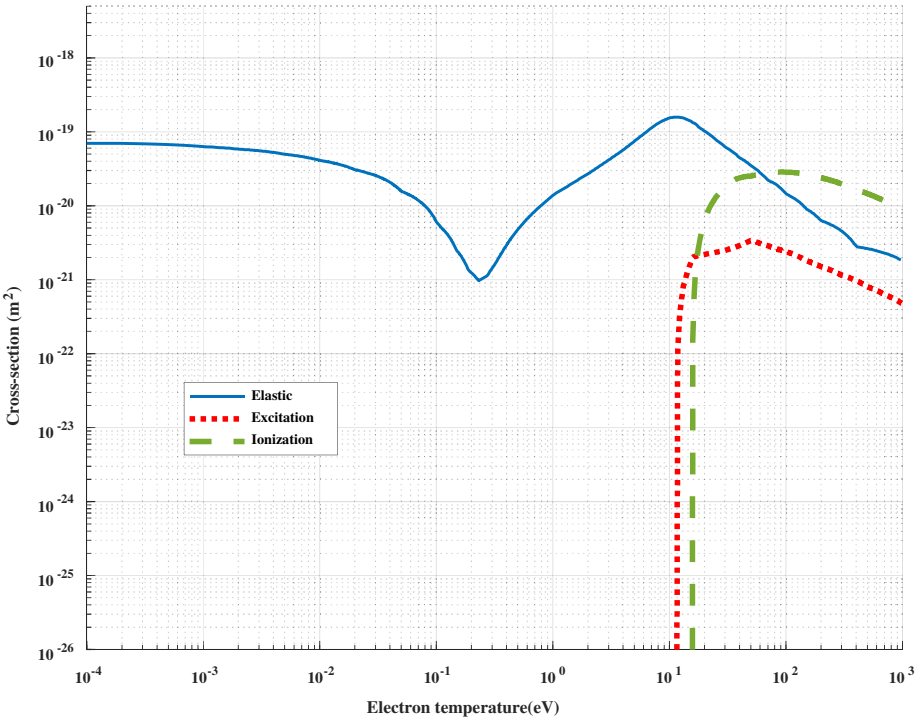

FIGURE 2. Cross-section (m^2) vs. Electron Temperature (eV) of Argon gas.

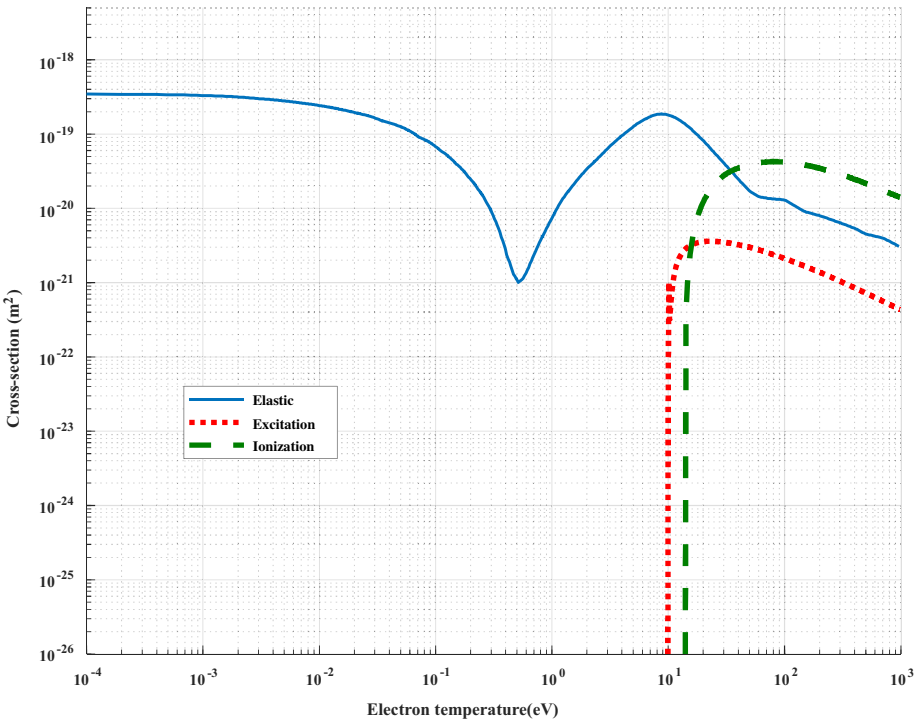

FIGURE 3. Cross-section (m^2) vs. Electron Temperature (eV) of Krypton gas.

V. The simulation of this model requires the cross-sections for electron-atom collisions, which can be obtained using the Boltzmann code BOLSIG [36]. By using this code, we plotted the cross-section as a function of T_e for different gases, as shown in Figures 2, 3, and 4.

Based on the results obtained, two distinct regions of electron temperature (T_e) can be identified for all three gases. In the first region, corresponding to low electron temperatures ($T_e \leq 10$ eV), the excitation and ionization cross sections are negligible compared to the elastic cross section. In the second region, where the electron temperature exceeds 10 eV ($T_e > 10$ eV), all

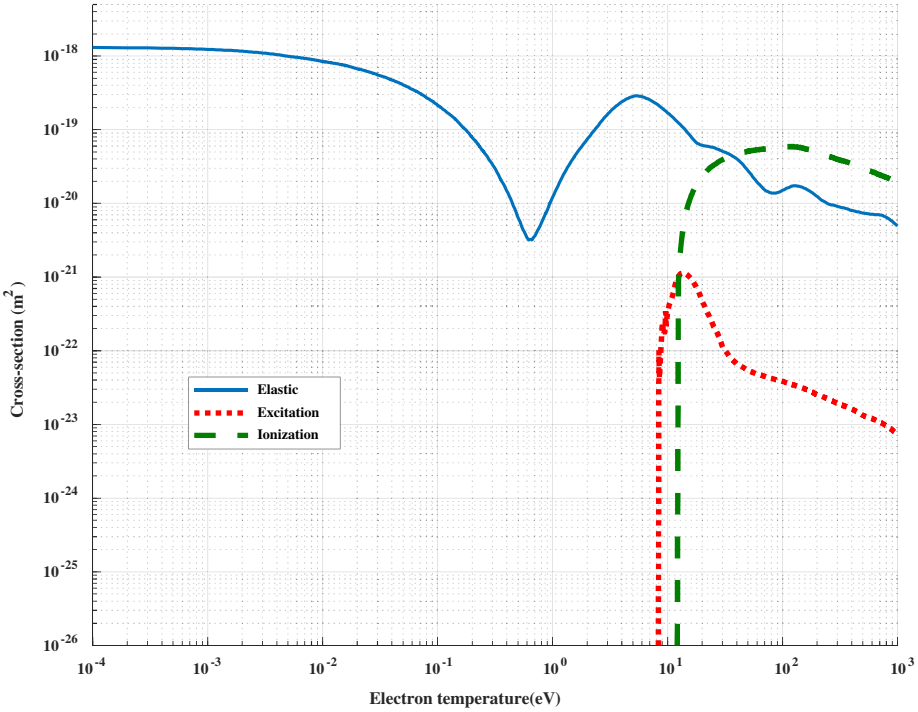

FIGURE 4. Cross-section (m^2) vs. Electron Temperature (eV) of Xenon gas.

three types of cross sections: elastic, excitation, and ionization must be taken into account.

If we consider a cold plasma, where the electrons have low energy (for example, below 10 eV), elastic scattering is the dominant interaction. This assumption can simplify the calculation, especially for the collision frequency in the plasma, which is given by the following expression [37]:

$$\upsilon_c = \sqrt{\frac{8}{\pi K m_e}} \left[(T_g) (P_g) \left(T_e^{0.5} \right) \left(Q_{e-a}^{elas} \right) \right] \tag{5}$$

Despite its simplicity, this new form of the formula is very convenient to use for cold plasma applications, since it only requires knowledge of the values of T_g, P_g, T_e, and Q_{e-a}^{elas}.

2.2.1. Governing Equations

The different plasmas considered in this model can be described by the continuity equations given below [38]

$$\frac{\partial(n_e)}{\partial t} + \nabla(\Gamma_e) = R_i N n_e \tag{6}$$

$$\frac{\partial(n_p)}{\partial t} + \nabla(\Gamma_p) = R_i N n_e \tag{7}$$

$$\frac{\partial(n_*)}{\partial t} + \nabla(\Gamma_*) = R_{ex} N n_e \tag{8}$$

where n_e, n_p, n_*, and N are the electron density, positive ion density, excited atom density, and neutral gas density, respectively. Γ_e, Γ_p, and Γ_* are the fluxes of electrons, positive ions, and excited atoms, respectively. R_i and R_{ex} are the ionisation and excitation rate coefficients, respectively. The index "j" represents the process index, and it can denote the ionization process (i) and excitation process (ex). The rate coefficients R_j for each process are defined by the following formula [36]:

$$R_j = \int_0^\infty f(\varepsilon)\sigma_i(\varepsilon)\upsilon(\varepsilon)d\varepsilon \tag{9}$$

where $f(\varepsilon)$ is the Electron Energy Distribution Function (EEDF), σ_i the collision cross-section, ε the electron energy, and υ the electron velocity.

2.2.2. Drift Diffusion Approach

To simplify the solution of the previous continuity equation, we used the drift-diffusion approximation based on particle flux. This flux is the superposition of particle drift due to an electric field and particle diffusion due to a density gradient. The drift term vanishes for excited atoms because they are neutral [38]:

$$\Gamma_e = -n_e \mu_e E - D_e \nabla n_e \tag{10}$$

$$\Gamma_p = -n_p \mu_p E - D_p \nabla n_p \tag{11}$$

$$\Gamma_* = 0 - D_* \nabla n_* \tag{12}$$

where μ_e and μ_p are the electron mobility and positive ion mobility, respectively. D_e, D_p, and D_* are the diffusion coefficients for electrons, ions, and excited atoms, respectively. E is the RF electric field. Based on the assumptions made at the beginning of Subsection 2.2, the energy equation is solved only for electrons as follows:

$$\frac{\partial(n_\varepsilon)}{\partial t} + \nabla(\Gamma_\varepsilon) = -\Gamma_\varepsilon E - S_\varepsilon \tag{13}$$

$$\Gamma_\varepsilon = -n_\varepsilon \varepsilon \mu_\varepsilon E - D_\varepsilon \nabla (n_\varepsilon) \quad (14)$$

$$n_\varepsilon = n_e < \varepsilon > \quad (15)$$

$$< \varepsilon > = \left(\frac{3}{2}\right) T_e \quad (16)$$

where n_ε is the electron energy density; Γ_ε is the mean electron energy flux; S_ε is the electron energy source; D_ε and μ_ε are the diffusion coefficient and electron mobility for the energy flux, respectively; $< \varepsilon >$ is the electron mean energy; and T_e is the electron temperature. Finally, to calculate the electric field in the plasma, Poisson's equation is needed to be solved simultaneously with the fluid equations as shown in the following formula:

$$\Delta V = -\frac{|q|}{\varepsilon_0} (n_p - n_e) \quad (17)$$

and

$$E = -\nabla V \quad (18)$$

where ΔV is the differential electrostatic potential, q the elementary charge of the electrons, and ε_0 the electrical permittivity in vacuum.

Due to the significant interconnection among all the previous plasma differential Equations (6)–(18), the solutions of the electron density or electron temperature equations are very complicated. For this reason, we have used the COMSOL Multiphisics software [39], which is based on the finite element method, to numerically solve these equations. The simulated plasma reactor was modeled using the following input parameters as presented in Table 4 below:

TABLE 4. Plasma input parameters.

	Value/Expression	Unit	Description
P_g	1.5	Torr	Gas pressure
T_g	300	Kelvin	Gas temperature
$V_{\max}$	2 KV	Volt	Maximum voltage
f_d	19000	Hz	Voltage frequency
V_{rf}	$V_{\max} \cos(2\pi f_d t)$	Volt	RF Discharge voltage

3. PLASMA AND EM WAVES INTERACTION

3.1. Drude Model

The Drude model [40] is a simplified description to study the behavior of plasma. It takes into account electrical permittivity, conductivity, and other properties to help understand how free electrons in plasma respond rapidly to internal or external electromagnetic fields. This model is used to describe how plasma interacts with an electromagnetic perturbation. In this model, the motion of electrons in the plasma medium can be described by a nonhomogeneous differential equation:

$$m_e \frac{\partial \vec{V_e}}{\partial t} = -e\vec{E} - m_e \nu_c \vec{V_e} \quad (19)$$

where m_e, $\vec{V_e}$, e, and $\vec{E}$ are the electron mass, electron velocity, elementary electric charge, and electric field, respectively, and ν_c is the collision frequency between the electron and neutral atom.

Combining the above Equation (19) and the Maxwell-Ampere equation [41], the relative plasma permittivity ε_p and electric plasma conductivity σ_p can be obtained using the following formula [40]:

$$\varepsilon_p = 1 - \frac{\left(\frac{\omega_p}{\omega}\right)^2}{1 + \left(\frac{\omega}{\nu_c}\right)^2} - j\frac{\left(\frac{\omega_p}{\omega}\right)^2 \left(\frac{\nu_c}{\omega}\right)}{1 + \left(\frac{\nu_c}{\omega}\right)^2} \quad (20)$$

$$\sigma_p = \varepsilon_0 \frac{\left(\frac{\omega_p}{\omega}\right)^2 \nu_c}{1 + \left(\frac{\nu_c}{\omega}\right)^2} - j\varepsilon_0 \frac{\left(\frac{\omega_p^2}{\omega}\right)}{1 + \left(\frac{\nu_c}{\omega}\right)^2} \quad (21)$$

where $\omega_p = \sqrt{\frac{e^2 n_e}{\varepsilon_0 m_e}}$ is the plasma frequency [40], ω the operating frequency, and n_e the electron density.

The Drude model was adopted for this study because the investigated discharges correspond to cold, weakly ionized, and unmagnetized plasmas. Under these specific conditions:

- Electrons undergo predominantly elastic collisions with neutral atoms, which far outweigh electron-ion and electron-electron interactions (negligible).
- The electron velocity distribution function remains close to a Maxwellian distribution [42], characteristic of a system near thermal equilibrium.
- These two properties allow the complete description of the plasma's electric behavior using only two parameters: the plasma frequency (ω_p) and the effective collision frequency (ν_c) [43].

Consequently, the Drude formulation accurately captures the complex permittivity and conductivity of the plasma over the entire investigated frequency range, while maintaining mathematical simplicity.

3.2. Theoretical Analysis of R and T under Plasma Sheath

In this work, the transmission and reflection characteristics of cold plasma are investigated using the TMM method, where the plasma medium is surrounded by air, as shown in Figure 5.

To avoid the distinctions between TM and TE modes in the expressions of the reflection and transmission coefficients, we have considered normal incidence, $\theta_i = 0°$ $(i = 1, 2, 3)$. In addition, we assumed that the plasma is an unmagnetized medium, which allows us to write: $\mu_p = \mu_0 = 1$. The amplitudes of the incident (A), reflected (B), and transmitted (F) electric fields on both sides of the plasma tubes can be expressed in the following form [22].

$$\begin{bmatrix} 1 & 1 \\ \eta_0 & -\eta_0 \end{bmatrix} \begin{bmatrix} A \\ B \end{bmatrix} = M \times F \begin{bmatrix} 1 \\ \eta_0 \end{bmatrix} \quad (22)$$

where M is the transfer matrix of plasma surrounded by air and is given by the following formula:

$$M = \begin{bmatrix} M_{11} & M_{12} \\ M_{21} & M_{22} \end{bmatrix} \quad (23)$$

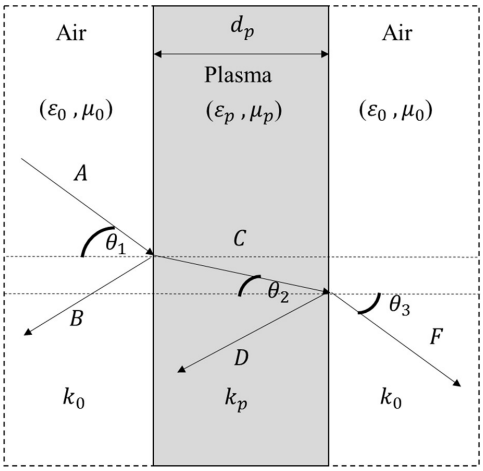

FIGURE 5. Schematic representation of plasma slab surrounded by air layers for TMM analysis.

with each M_{ij} given by:

$$M_{11} = \cos\left(\frac{\omega}{c} d_p \sqrt{\varepsilon}_p \cos(\theta_2)\right) \quad (24)$$

$$M_{12} = \frac{j}{\eta_p} \sin\left(\frac{\omega}{c} d_p \sqrt{\varepsilon}_p \cos(\theta_2)\right) \quad (25)$$

$$M_{21} = j\eta_p \sin\left(\frac{\omega}{c} d_p \sqrt{\varepsilon}_p \cos(\theta_2)\right) \quad (26)$$

$$M_{22} = \cos\left(\frac{\omega}{c} d_p \sqrt{\varepsilon}_p \cos(\theta_2)\right) \quad (27)$$

where d_p is the width of the plasma medium, and η_i is the impedance of the plasma given by:

for TE modes

$$\eta_{pTE} = \eta_{0TE} \sqrt{\varepsilon}_p \cos(\theta_2) \text{ where } \eta_{0TE} = \sqrt{\frac{\varepsilon_0}{\mu_0}} \quad (28)$$

for TM modes

$$\eta_{pTM} = \left(\eta_{0TM} \sqrt{\varepsilon}_p\right)^{-1} \cos(\theta_2) \text{ where } \eta_{0TM} = \sqrt{\frac{\mu_0}{\varepsilon_0}} \quad (29)$$

and k_p is the propagation constant in the plasma and is given by:

$$k_p = \frac{\omega}{c} \sqrt{\varepsilon}_p = k^{'} + ik^{''} \quad (30)$$

where $k^{'}$ and $k^{''}$ are the attenuation coefficient and phase-shift coefficient, respectively, and are expressed by:

$$k' = \frac{\omega}{c} \left\{ -\frac{1}{2} \cdot \left(1 - \frac{\omega_p^2}{\omega^2 + \nu_c^2}\right) + \frac{1}{2} \cdot \left[\left(1 - \frac{\omega_p^2}{\omega^2 + \nu_c^2}\right)^2 + \left(\frac{\nu_c^2}{\omega^2}\right)^2 \cdot \left(\frac{\omega_p^2}{\omega^2 + \nu_c^2}\right)^2 \right]^{1/2} \right\}^{1/2} \quad (31)$$

$$k'' = \frac{\omega}{c} \left\{ \frac{1}{2} \cdot \left(1 - \frac{\omega_p^2}{\omega^2 + \nu_c^2}\right) + \frac{1}{2} \cdot \left[\left(1 - \frac{\omega_p^2}{\omega^2 + \nu_c^2}\right)^2 + \left(\frac{\nu_c^2}{\omega^2}\right)^2 \cdot \left(\frac{\omega_p^2}{\omega^2 + \nu_c^2}\right)^2 \right]^{1/2} \right\}^{1/2} \quad (32)$$

From the expression of Equation (23), we can deduce the expression of the complex amplitudes of reflection (r) and transmission (t) coefficients of unmagnetized cold plasma surrounded by two vacuum layers as follows:

$$r = \frac{j \sin(k_p d_p) \left[\frac{\eta_0}{\eta_p} - \frac{\eta_p}{\eta_0}\right]}{2\cos(k_2 d_p) + i \sin(K_p d_p) \left[\frac{\eta_0}{\eta_p} + \frac{\eta_p}{\eta_0}\right]} \quad (33)$$

$$t = \frac{2}{2\cos(k_p d_p) + j \sin(k_p d_p) \left[\frac{\eta_0}{\eta_p} + \frac{\eta_p}{\eta_0}\right]} \quad (34)$$

and the reflection (R), transmission (T), and absorption (A) powers are given by:

$$R = |r|^2 \quad (35)$$

$$T = |t|^2 \quad (36)$$

$$A = 1 - (R + T) \quad (37)$$

From these equations, we can see that the reflection, transmission, and absorption coefficients of the plasma depend on ω, ω_p, d_p, and ν_c. By changing these parameters, we can control the response of plasma to electromagnetic waves, i.e., we can force the plasma to behave as either a transparent, dissipative, or reflective medium.

4. RESULTS AND DISCUSSIONS

4.1. Plasma and Collision Frequency

In this study, we have considered the operating frequency range from 0 GHz to 200 GHz to cover almost all frequency band applications. We have set the plasma diameter to d_p= 6 mm (Section 2) so that the reflection (R) and transmission (T) coefficients on the plasma depend only on ω_p and ν_c, which are the intrinsic parameters for the three gases. We then simulated this model for three types of gases using COMSOL Multiphysics, and the obtained results are shown in Table 5.

From these results, it can be noticed that the values of the parameters depend on the type of gas used, even though the same discharge conditions were applied. The electron density obtained for argon gas, approximately 4.6×10^{18} m^{-3}, is close to the experimental value reported by Melazzi et al. [10]. Unfortunately, comparisons with experimental results for krypton and xenon under the same conditions could not be performed due to the lack of experimental data for these gases. Notably, the electron temperature values for the considered gases are still below 10 eV, which allows us to use the simplified formula (5) to calculate the collision frequency of the electrons inside the plasma.

TABLE 5. Different parameters of plasma medium for different gases.

Gas type	$n_{e(}m_{)}^{-3}$	$\omega_p(rads^{-1})$	$f_p(GHz)$	T_e (eV)	$Q_{e-a}(m^2)$	υ_c (Hz)
Argon	4.687×10^{18}	1.221×10^{11}	~ 20	1.006	$\sim1.38\times10^{-20}$	4.5×10^{8}
Krypton	9.051×10^{19}	5.365×10^{11}	~ 85	0.841	$\sim4.38\times10^{-21}$	1.3×10^{8}
Xenon	2.453×10^{20}	8.833×10^{11}	~ 140	0.9949	$\sim0.65\times10^{-21}$	8.4×10^{8}

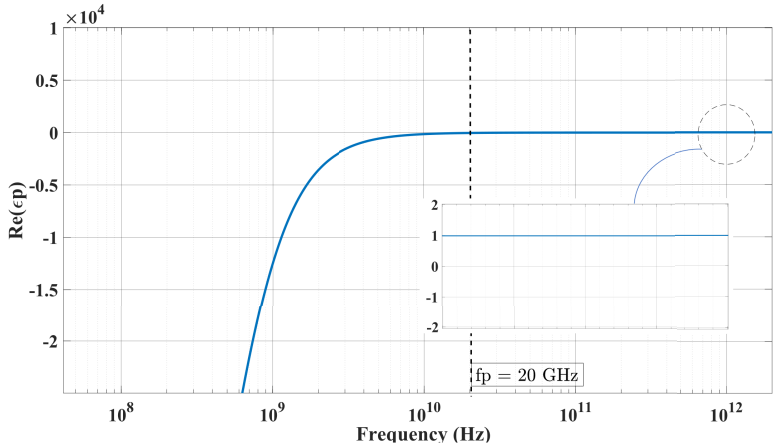

FIGURE 6. Real part of argon electrical permittivity as a function of frequency.

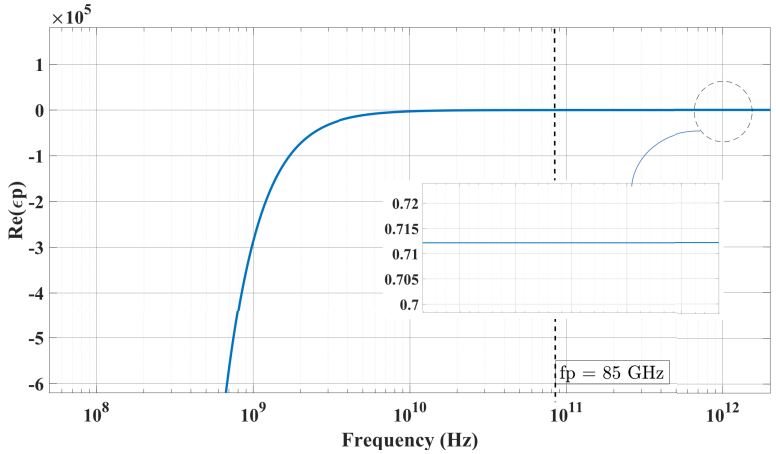

FIGURE 7. Real part of krypton electrical permittivity as a function of frequency.

4.2. Electric Permittivity for Different Gases

The electrical permittivity of the plasma characterizes the ability of free electrons to respond to an oscillating electric field. To analyze how permittivity varies with the type of gas considered, we used Equation (20) to plot the real part of the plasma permittivity for different gases, as illustrated in Figures 6, 7, and 8. These plots reveal that, depending on the frequency of the incident electromagnetic wave, the plasma exhibits two distinct behaviors:

i. Reflective behavior in the low frequency range ($\omega \ll \omega_p$):

When the frequency of the incident wave is much lower than the plasma frequency, the electrons can effectively follow the oscillations of the electric field, resulting in the reflection of the electromagnetic wave. Mathematically, this corresponds to a negative real part of permittivity ($\mathrm{Re}(\varepsilon_p) < 0$), indicating that the plasma acts as a mirror for the incoming waves.

ii. Transparency behavior in the high frequency range ($\omega \gg \omega_p$):

On the other hand, when the frequency of the incident wave is much higher than the plasma frequency, the electrons are unable to respond to the rapid oscillations of the electric field. Consequently, the wave propagates through the plasma with minimal interaction. In this case, the real part of permittivity becomes positive ($\mathrm{Re}(\varepsilon_p) > 0$), indicating that the plasma behaves like a dielectric medium.

By analyzing the results in Figure 6, it is clear that the transition from reflective (negative permittivity) to transparent (pos-

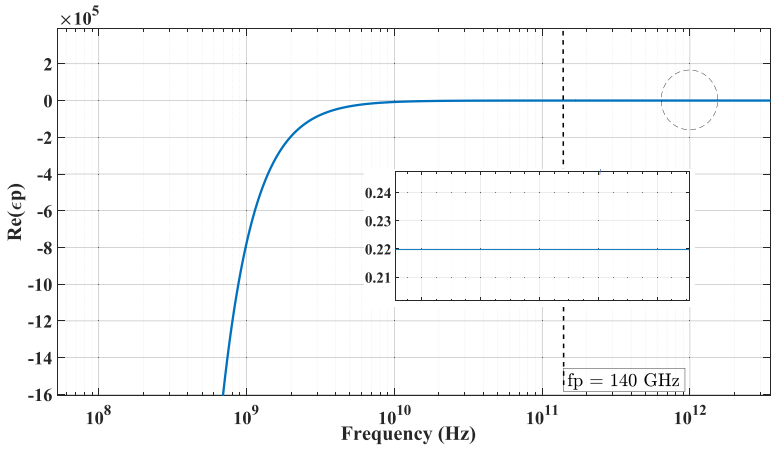

FIGURE 8. Real part of xenon electrical permittivity as a function of frequency.

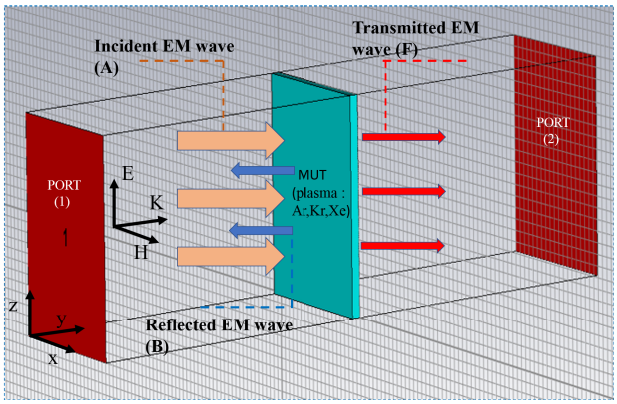

FIGURE 9. MUT (plasma slab) between two parallel plane wave ports.

itive permittivity) state for the argon gas occurred earlier than krypton and xenon gases (Figures 7 and 8). It means that argon reflects waves at a lower frequency ($\ll 20$ GHz) than the other gases. While the frequency increases, argon gradually becomes dielectric, with permittivity approaching 1.

Krypton, with its higher plasma frequency (85 GHz), behaves as a reflective medium over a longer frequency range before transitioning to transparency, as shown in Figure 7. Krypton also behaves as a dielectric medium at high frequencies.

Figure 8 shows that xenon, which has the highest plasma frequency (140 GHz), reflects waves for the widest frequency range. The transition to wave propagation happens only at much higher frequencies than both argon and krypton. In the ultra-high-frequency range, xenon eventually behaves as a dielectric, with permittivity beginning to approach 1, and this happens much later than in argon or krypton.

4.3. Reflection and Transmission Coefficient Using TMM

The calculation of power reflection (R) and transmission (T) coefficients using TMM is critical in evaluating the gases, such as argon, krypton, and xenon, to determine if they can be used as plasma reflectors or transmitters depending on the application. The ability to fine-tune these coefficients underscores the potential of plasma technology to create adaptive systems that can be tailored to specific needs in different frequency bands.

The TMM calculation results were validated against FDTD using the Computer Simulation Technology (CST) software [45], which is based on the FDTD method. In CST, we have modeled a plasma slab (Figure 9) with the same parameters used above in TMM calculations: d_p, ω_p, and υ_c. The obtained results, for different gases, are presented in Figures 10(a), 11(a), and 12(a), where the reflection and transmission coefficients obtained by the TMM and the CST/FDTD solver exhibit an almost perfect overlap throughout the investigated frequency range (0–200 GHz). This agreement demonstrates that the two independent methods capture the same electromagnetic response of the plasma slab. In addition to this numerical validation, TMM is significantly faster than FDTD simulation. TMM approach computes the full broadband response within only a few seconds, while the CST/FDTD simulation requires several hours depending on the mesh density and boundary setup (Table 6). This disparity arises because TMM directly solves frequency-domain transfer relations, whereas CST/FDTD simulation performs time-stepping over the entire spatial grid followed by Fourier transformation. Consequently, TMM is particularly advantageous for wideband parametric studies, whereas CST/FDTD simulation remains useful for validating the field distribution and transient phenomena.

By analyzing Figures 10, 11, and 12 for the gases considered, we see that there are three important areas where

1) When $\omega < \omega_p$:

   The coefficient of reflection (R) is near 1, whilst the coefficient of transmission (T) is weak and near 0. In this case, the plasma serves the purpose of a good reflector of electromagnetic waves.

2) When $\omega \approx \omega_p$:

   When the frequency of the incoming wave ω is nearly the same as the plasma frequency ω_p, resonance phenomena occur, and the plasma shows anomalous behavior, written as a negative absorption coefficient ($A < 0$), which falls off as we depart further from the plasma frequency.

3) When $\omega \gg \omega_p$:

TABLE 6. Quantitative comparison between two methods, TMM and CST/FDTD.

Method	Simulation Type	Frequency Range	Computation Time
TMM	Analytical/Frequency domain	0–200 GHz	< 10 s
CST FDTD	Full-wave/Time-Domain	0–200 GHz	∼5–10 h (depending on mesh size 20–40 celles/λ)

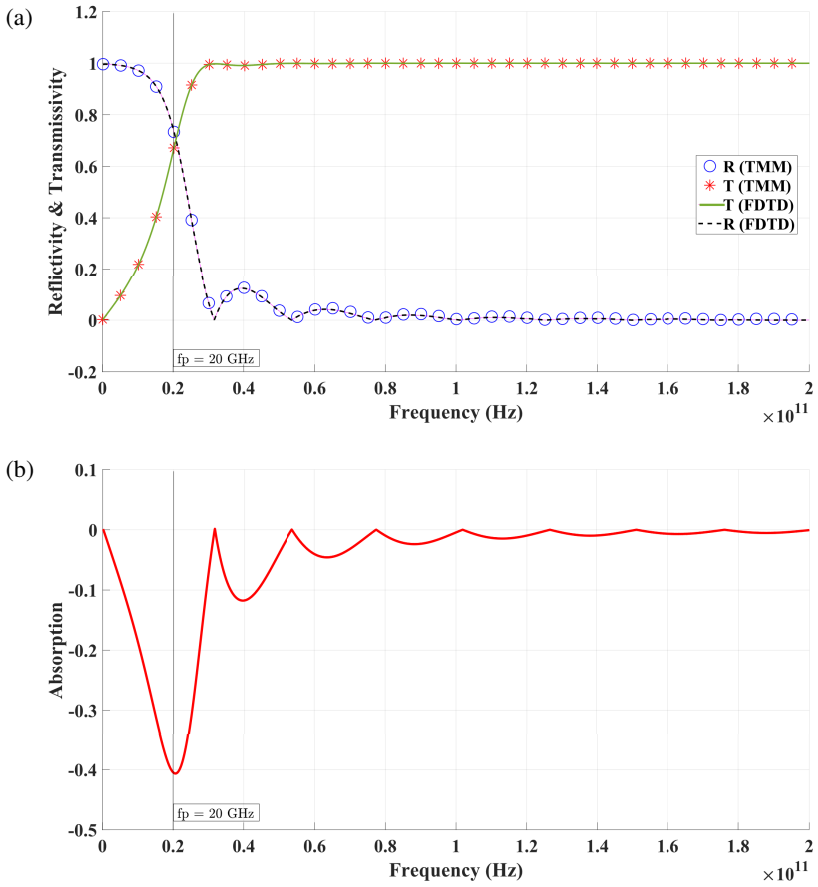

FIGURE 10. Argon: (a) Reflection and transmission coefficient; (b) Absorption coefficient.

When the frequency of the incoming wave ω is very large compared with the frequency of the plasma ω_p, the coefficient of reflection (R) decreases to a low value, whilst that of transmission (T) increases to a value near 1. In this case, the plasma serves as a good transmitter of electromagnetic waves.

The frequency-dependent behavior obtained in Figures 10–12, characterized by a reflective regime for $\omega < \omega_p$ and a transmissive regime for $\omega > \omega_p$, is consistent with several experimental observations reported for rare-gas plasmas. Experimental microwave diagnostics of argon discharges have shown a strong reflection below the plasma frequency and increased transmission above it [46]. Likewise, reflectivity measurements of shock-compressed xenon plasmas demonstrate a sharp transition from metallic to transparent behaviour as the probing frequency exceeds ω_p [45]. Comparative discharge studies for krypton and xenon [46] confirm electron densities that place their plasma frequencies in the microwave-millimetre range, consistent with the transition observed near 85 GHz in Figure 11. Additionally, a qualitative comparison with other works [26] and [48], when $\omega \approx \omega_p$, reveals anomalous behaviour, where ($R + T > 1$) shows a negative absorption ($A < 0$) due to high temperature plasma. In our case, the negative absorption is due to the resonance phenomenon that happens when the wave frequency is close to the plasma frequency f_p as shown in Figures 10(b), 11(b), and 12(b). Near the plasma frequency, the plasma may contribute energy to the wave rather than dissipating it [49, 50]. These consistent experimental findings qualitatively validate the numerical trends presented in this work.

As a result of the previous analyses, argon can be used as a good reflector in the frequency range under 20 GHz. In contrast, krypton can be used as a good reflector in a frequency range greater than argon, from 0 to 85 GHz. While xenon plays the role of a reflector from 0 GHz to 140 GHz, which is higher than argon and krypton. We can consider that argon is a better transmitter of electromagnetic waves than krypton and xenon, because the transmission behavior of argon shows good stabil-

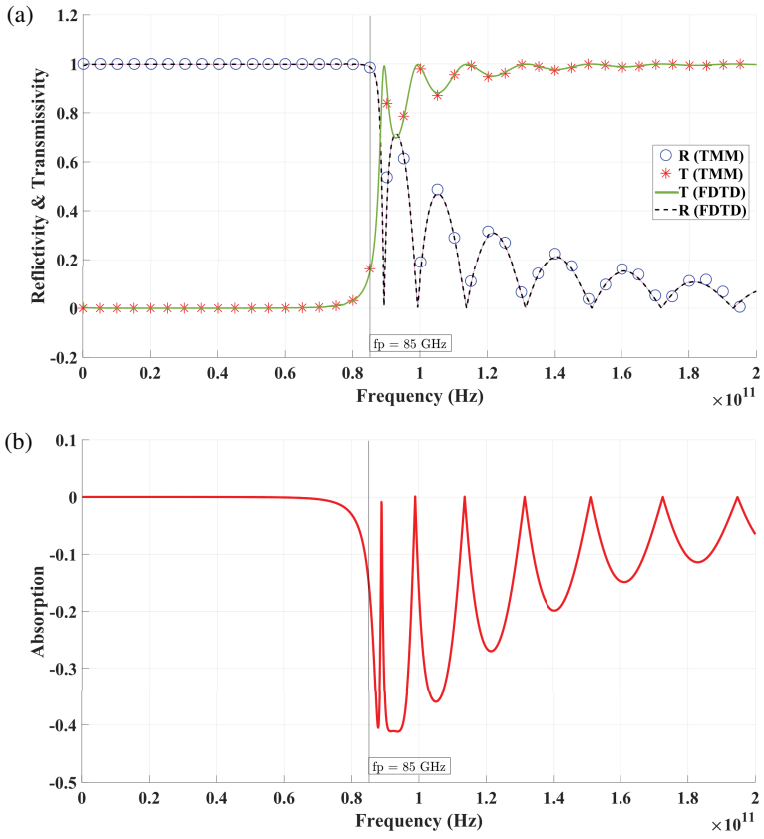

FIGURE 11. Krypton: (a) Reflection and transmission coefficient; (b) Absorption coefficient.

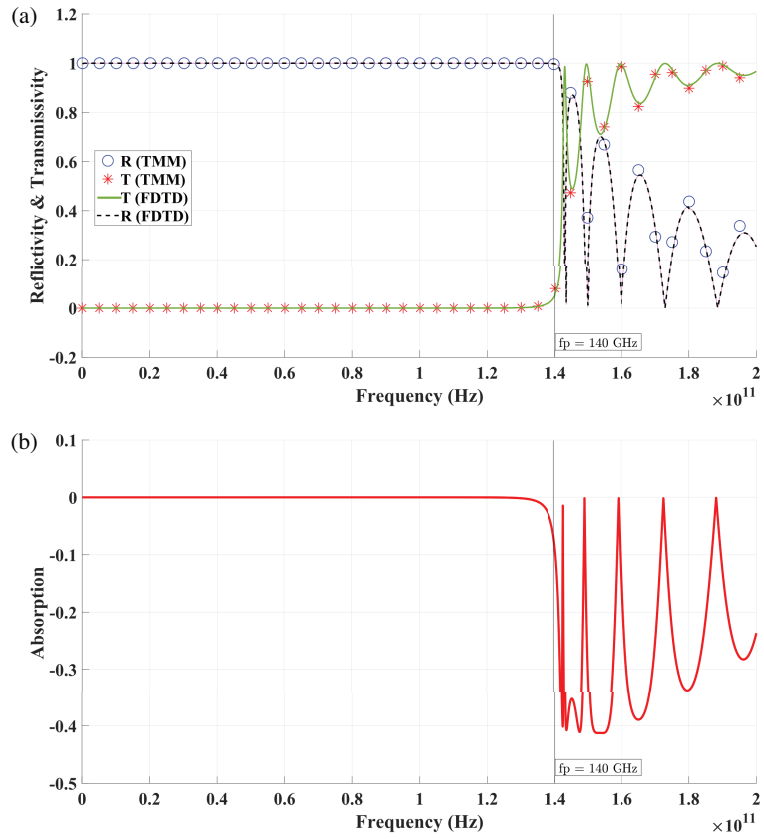

FIGURE 12. Xenon: (a) Reflection and transmission coefficient; (b) Absorption coefficient.

ity compared to the previous gases that suffer from the problem of anomalous behavior at resonance. In addition, argon plays the role of a good transmitter in a wider frequency range than krypton and xenon, starting from about 30 GHz to 200 GHz.

5. CONCLUSION

The frequency-dependent electromagnetic interactions of argon, krypton, and xenon plasmas are studied systematically in the present work, using a combined fluid approach, Drude model, and transfer matrix method (TMM). The electron density and collisional frequency have been obtained from a one-dimensional fluid dynamic model operated in COMSOL Multiphysics, and the resulting values have been used to evaluate the reflection and transmission coefficients in the frequency range 0–200 GHz. Analysis shows the existence of different reflection and transmission regimes for each gas considered, with argon being a good reflector in frequencies below 20 GHz and practically transparent above 30 GHz, krypton being a very good reflector to about 85 GHz, and xenon being a very good reflector to about 140 GHz before it becomes transmissive. These variations in electromagnetic response are due to differences in the values of the plasma frequency and the electron-neutral collision rates of the considered gases. Such findings illustrate that the electromagnetic response of plasmas changes according to their composition. A detailed discussion of the advantages of the TMM, as against the FDTD simulation using CST, for the general broadband analysis of plasmas is given. A comparison between the two methods, satisfactory with respect to results for transmission and reflection coefficients, is noted in which the time of computation for the TMM method is found to be much shorter (from several hours in the case of the CST/FDTD simulation to seconds with the TMM method) with no loss of accuracy. A very useful property of the TMM method is that it allows the very rapid, wideband analysis of electromagnetic structures utilizing plasmas to be made with a view to preliminary design optimization before the tedious full-wave FDTD analysis.

Future work would then have to concentrate on adding further layers, e.g., the chamber, to move from a theoretical model to a more realistic representation of the plasma reflector system, and perform experimental verifications, which would utilize the full possibilities offered by plasma reflectors, plasma antennas, intelligent reflective surfaces (IRS), and other reconfigurable electromagnetic structures in practical applications.

REFERENCES

[1] Tonks, L. and I. Langmuir, "Oscillations in ionized gases," *Physical Review*, Vol. 33, No. 2, 195, 1929.

[2] Petrin, A. B., "Transmission of microwaves through magnetoactive plasma," *IEEE Transactions on Plasma Science*, Vol. 29, No. 3, 471–478, 2001.

[3] Kumar, R. and D. Bora, "Wireless communication capability of a reconfigurable plasma antenna," *Journal of Applied Physics*, Vol. 109, No. 6, 063303, Mar. 2011.

[4] Zhao, J., Y. Chen, Y. Sun, H. Wu, Y. Liu, and Q. Yuan, "Plasma antennas driven by 5–20 kHz AC power supply," *AIP Advances*, Vol. 5, No. 12, 127114, Dec. 2015.

[5] Naito, T., S. Yamaura, Y. Fukuma, and O. Sakai, "Radiation characteristics of input power from surface wave sustained plasma antenna," *Physics of Plasmas*, Vol. 23, No. 9, 093504, Sep. 2016.

[6] Sadeghikia, F., A. K. Horestani, M. T. Noghani, M. R. Dorbin, H. Mahdikia, and H. Ja'afar, "A study on the effect of the radius of a cylindrical plasma antenna on its radiation efficiency," *International Journal of Engineering and Technology*, Vol. 7, 204–206, 2018.

[7] Ye, H. Q., M. Gao, and C. J. Tang, "Radiation theory of the plasma antenna," *IEEE Transactions on Antennas and Propagation*, Vol. 59, No. 5, 1497–1502, 2011.

[8] Alexeff, I., T. Anderson, E. Farshi, N. Karnam, and N. R. Pulasani, "Recent results for plasma antennas," *Physics of Plasmas*, Vol. 15, No. 5, 057104, 2008.

[9] Jusoh, M. T., O. Lafond, F. Colombel, and M. Himdi, "Performance and radiation patterns of a reconfigurable plasma corner-reflector antenna," *IEEE Antennas and Wireless Propagation Letters*, Vol. 12, 1137–1140, 2013.

[10] Melazzi, D., P. D. Carlo, F. Trezzolani, M. Manente, A.-D. Capobianco, and S. Boscolo, "Beam-forming capabilities of a plasma circular reflector antenna," *IET Microwaves, Antennas & Propagation*, Vol. 12, No. 15, 2301–2306, Dec. 2018.

[11] Sadeghikia, F., M. Valipour, M. T. Noghani, H. Ja'afar, and A. K. Horestani, "3d beam steering end-fire helical antenna with beamwidth control using plasma reflectors," *IEEE Transactions on Antennas and Propagation*, Vol. 69, No. 5, 2507–2512, May 2021.

[12] Wang, H., X. Lyu, J. Yao, A. M. Astafiev, and H.-P. Li, "Study of the radiation pattern and frequency response of a short linear antenna surrounded by discharge tubes for the development of rapidly adjustable wideband antenna systems," *Electronics*, Vol. 12, No. 6, 1277, Mar. 2023.

[13] Yuan, J., T. Ning, H. Li, L. Pei, J. Li, J. Zheng, and L. Wan, "Terahertz filters based on subwavelength polymer waveguide," *Results in Physics*, Vol. 13, 102198, Jun. 2019.

[14] Luo, S., J. E. Scharer, M. Thiyagarajan, and C. M. Denning, "Experimental study of laser-initiated radiofrequency-sustained high-pressure plasmas," *IEEE Transactions on Plasma Science*, Vol. 34, No. 6, 2637–2651, 2006.

[15] Conrads, H. and M. Schmidt, "Plasma generation and plasma sources," *Plasma Sources Science and Technology*, Vol. 9, No. 4, 441, 2000.

[16] Moisan, M., A. Shivarova, and A. W. Trivelpiece, "Experimental investigations of the propagation of surface waves along a plasma column," *Plasma Physics*, Vol. 24, No. 11, 1331, 1982.

[17] Vollmer, M. and K.-P. Möllmann, *Infrared Thermal Imaging: Fundamentals, Research and Applications*, John Wiley & Sons, 2018.

[18] Chang, C.-W., M. Davoudabadi, and F. Mashayek, "One-dimensional fluid model of methane plasma for diamond-like coating," *IEEE Transactions on Plasma Science*, Vol. 38, No. 7, 1603–1614, Jul. 2010.

[19] Cummer, S. A., "An analysis of new and existing FDTD methods for isotropic cold plasma and a method for improving their accuracy," *IEEE Transactions on Antennas and Propagation*, Vol. 45, No. 3, 392–400, 1997.

[20] Yuan, C.-X., Z.-X. Zhou, J. W. Zhang, X.-L. Xiang, F. Yue, and H.-G. Sun, "FDTD analysis of terahertz wave propagation in a high-temperature unmagnetized plasma slab," *IEEE Transactions on Plasma Science*, Vol. 39, No. 7, 1577–1584, Jul. 2011.

[21] Zhang, Y., Y. Liu, and X. Li, "A 2-D FDTD model for analysis of plane wave propagation through the reentry plasma sheath,"

IEEE Transactions on Antennas and Propagation, Vol. 65, No. 11, 5940–5948, Nov. 2017.

[22] Chen, W., L. Guo, J. Li, and S. Liu, "Research on the FDTD method of electromagnetic wave scattering characteristics in time-varying and spatially nonuniform plasma sheath," *IEEE Transactions on Plasma Science*, Vol. 44, No. 12, 3235–3242, Dec. 2016.

[23] Yuan, C. X., Z. X. Zhou, and H. G. Sun, "Reflection properties of electromagnetic wave in a bounded plasma slab," *IEEE Transactions on Plasma Science*, Vol. 38, No. 12, 3348–3355, Dec. 2010.

[24] Hu, B. J., G. Wei, and S. L. Lai, "SMM analysis of reflection, absorption, and transmission from nonuniform magnetized plasma slab," *IEEE Transactions on Plasma Science*, Vol. 27, No. 4, 1131–1136, 1999.

[25] Yang, M., X. Li, B. Bai, Z. Li, and B. Xue, "Transmission coefficient estimation based on antenna voltage standing wave ratio under plasma sheath," *AIP Advances*, Vol. 8, No. 7, 075018, Jul. 2018.

[26] Liu, J.-X., W.-C. Tang, Y. Jiang, L. Ju, and H.-W. Yang, "A study of frequency selection characteristics of negative conductivity in high temperature plasma," *Results in Physics*, Vol. 14, 102467, 2019.

[27] Fu, G., S. Zhou, and L. Qi, "On the strain gradient elasticity theory for isotropic materials," *International Journal of Engineering Science*, Vol. 154, 103348, 2020.

[28] Fu, G., Z. Zhang, C. Dong, Y. Sun, J. Wang, and H. Zheng, "On the magneto-mechanical response of piezomagnetic microbeam with size effects," *Thin-Walled Structures*, Vol. 191, 111040, 2023.

[29] Fu, G., K. Jin, W. Song, S. Zhou, and H. Zheng, "On the nonclassical transfer matrix method for free vibration behaviour of multi-rigid-elastic unit microsystem," *Applied Mathematical Modelling*, Vol. 151, 116407, 2026.

[30] Lieberman, M. A. and A. J. Lichtenberg, "Principles of plasma discharges and materials processing," *MRS Bulletin*, Vol. 30, No. 11, 899–901, 2005.

[31] Colonna, G. and A. D'Angola, *Plasma Modeling: Methods and Applications*, IOP Publishing, 2022.

[32] Chung, T. H., H. S. Yoon, and J. K. Lee, "Scaling laws verification for capacitive rf-discharge ar plasma using particle-in-cell simulations," *Journal of Applied Physics*, Vol. 78, No. 11, 6441–6447, 1995.

[33] Kim, H.-Y., D.-C. Kwon, N.-S. Yoon, H.-H. Choe, and J.-H. Kim, "Development of new method for fluid simulation of capacitivelycoupled plasma discharge," *Journal of the Korean Physical Society*, Vol. 49, No. 51, 1967–1971, 2006.

[34] Kortshagen, U. and B. G. Heil, "Kinetic two-dimensional modeling of inductively coupled plasmas based on a hybrid kinetic approach," *IEEE Transactions on Plasma Science*, Vol. 27, No. 5, 1297–1309, 1999.

[35] Gudmundsson, J. T. and M. A. Lieberman, "Magnetic induction and plasma impedance in a cylindrical inductive discharge," *Plasma Sources Science and Technology*, Vol. 6, No. 4, 540, 1997.

[36] Boltzmann Solver for the SIGLO Series 1.0 ∼CPA Toulouse Kinema Software, 1996.

[37] El jaouhari, A., M. Rochdi, and M. E. Kaouini, "Effect of discharge parameters on conductive behavior and characteristics of monopole plasma antenna," *Materials Today: Proceedings*, Vol. 72, 3863–3868, 2023.

[38] Lymberopoulos, D. P. and D. J. Economou, "Fluid simulations of glow discharges: Effect of metastable atoms in argon," *Journal of Applied Physics*, Vol. 73, No. 8, 3668–3679, 1993.

[39] COMSOL, "COMSOL Multiphysics® v6.2."

[40] Tonks, L., "Oscillations in ionized gases," 122–139, 1961.

[41] Huray, P. G., *Maxwell's Equations*, John Wiley & Sons, 2009.

[42] Haas, F. A., A. Goodyear, and N. S. J. Braithwaite, "Tailoring of electron energy distributions in low temperature plasmas," *Plasma Sources Science and Technology*, Vol. 7, No. 4, 471, 1998.

[43] Wang, Y., C. Yuan, Z. Zhou, L. Li, and Y. Du, "Propagation of gaussian laser beam in cold plasma of drude model," *Physics of Plasmas*, Vol. 18, No. 11, 113105, 2011.

[44] CST Studio Suite, "CST Microwave Studio®," 2024.

[45] Bogdanov, E. N., M. V. Zhernokletov, G. A. Kozlov, and A. V. Rodionov, "Study of shock-compressed argon plasma using microwave diagnostics," *Combustion, Explosion, and Shock Waves*, Vol. 56, No. 4, 479–485, 2020.

[46] Reinholz, H., Y. Zaporoghets, V. Mintsev, V. Fortov, I. Morozov, and G. Röpke, "Frequency-dependent reflectivity of shock-compressed xenon plasmas," *Physical Review E*, Vol. 68, No. 3, 036403, 2003.

[47] Bethke, G. W. and A. D. Ruess, "Microwave reflection from shock-produced plasmas," *Physics of Fluids*, Vol. 7, No. 9, 1446–1455, 1964.

[48] Yuan, C., Z. Zhou, X. Xiang, H. Sun, H. Wang, M. Xing, and Z. Luo, "Propagation properties of broadband terahertz pulses through a bounded magnetized thermal plasma," *Nuclear Instruments and Methods in Physics Research Section B: Beam Interactions with Materials and Atoms*, Vol. 269, No. 1, 23–29, 2011.

[49] Twiss, R. Q., "Radiation transfer and the possibility of negative absorption in radio astronomy," *Australian Journal of Physics*, Vol. 11, No. 4, 564–579, 1958.

[50] Kruer, W., *The Physics of Laser Plasma Interactions*, CRC Press, 2019.